Quantum nonlinear planar Hall effect in bilayer graphene: An orbital effect of a steady in-plane magnetic field

N. Kheirabadi [*] and A. Langari [†]
Department of Physics, Sharif University of Technology, P.O.Box 11155-9161, Tehran, Iran

(Received 25 August 2022; revised 2 December 2022; accepted 20 December 2022; published 28 December 2022)

We study the quantum nonlinear planar Hall effect in bilayer graphene under a steady in-plane magnetic field. When time-reversal symmetry is broken by the magnetic field, a charge current occurs in the second-order response to an external electric field as a result of the Berry curvature dipole in momentum space. We show that a nonlinear planar Hall effect originating from the anomalous velocity is caused by an orbital effect of an in-plane magnetic field on electrons in bilayer graphene in the complete absence of spin-orbit coupling. Taking into account the symmetry analysis, we derive the dominant dependence of the Berry curvature dipole moment on the magnetic field components. Moreover, we illustrate how to control and modulate the Berry curvature dipole with an external planar magnetic field, gate voltage, and Fermi energy.

DOI: 10.1103/PhysRevB.106.245143

I. INTRODUCTION

During the last century, the Hall effect has played an important role in the advance of technology and condensed matter physics [1], and because of its profound relation to topology, the family of Hall effects has been diligently scrutinized in recent years [2–5].

When an electric field drives a current through a crystal, the system is out of equilibrium, and the electron velocity originates from the group velocity of the electron wave packet, while the anomalous velocity arises from the Berry curvature, which is an intrinsic property emerging from the band structure. The conventional Hall conductivity, the quantization of the Hall conductance in strong magnetic fields, can be considered the zero-order moment of the Berry curvature over occupied states [5]. The linear anomalous Hall effect and quantum anomalous Hall effect were recently observed in topological materials with broken time-reversal symmetry, such as magnetically doped topological insulators [6–8] and magnetic Weyl semimetals [9–11].

The first-order moment of the Berry curvature over the occupied states is defined by the Berry curvature dipole (BCD), which is a pseudotensor leads to the quantum nonlinear Hall effect [5]. It has been shown that up to second order and dissimilar to the linear effects, the quantum nonlinear Hall effect shows a component of the voltage oscillating at twice the frequency of the driving alternating electric field (the second-harmonic Hall voltage) and a steady component that is the result of the rectification effect, by which an AC electric field is turned into a DC signal [5]. The quantum nonlinear Hall effect has been distinguished in $1T_d$-WTe_2 [1,12,13] and has been predicted to occur in some developing materials with low crystalline symmetries [5,11,14]. For two-dimensional crystals with trigonal symmetry in the presence of in-plane magnetic field, a nonzero BCD also leads to a topological response in the nonlinear planar Hall effect [15].

In the planar Hall effect (PHE), in contrast to the ordinary Hall effect, the transverse voltage arises when an in-plane magnetic field is applied. In this regime, the applied electric field, the magnetic field, and the transverse Hall voltage are in the same plane, in contrast to the arrangement in which the conventional Hall effect vanishes. In most two-dimensional (2D) materials, the PHE has an absolutely semiclassical origin. In thin films of antiferromagnetic semiconductors, the observed PHE is suggested to be the result of band anisotropies [16]. It has also been indicated that PHE appears in 2D electron gases on the interfaces of perovskite oxides [17,18] and thin films of ferromagnetic semiconductors [19–21]. Moreover, the PHE performs an important role in the transport properties of Weyl semimetals. Recently, it was shown that the Zeeman-induced nontrivial Berry curvature affects the PHE in 2D trigonal crystals [15]. However, the common aspect of all of these cases is that the PHE arises from magnetic materials or spin-orbit origins.

In time-reversal-invariant materials, BCD is the effect of spin-orbit coupling or warping of the Fermi surface [22]. The quantum nonlinear planar Hall effect (QNLPHE) we discuss here is determined by BCD when time-reversal symmetry is broken by an applied in-plane magnetic field. This QNLPHE has a quantum effect arising from the anomalous velocity of Bloch electrons generated by the Berry curvature, which is not quantized [5]. In this study, we show that a nonzero BCD is achievable in the complete absence of spin effects in bilayer graphene, an excellent 2D material candidate with giant intrinsic carrier mobilities and a tunable band gap [23,24]. In addition, our results represent a distinct theoretical demonstration of a BCD which can be manipulated by magnetic fields. Such a tunable BCD leads to a broad range of quantum geometrical phenomena such as the magnetically switchable circular photogalvanic effect [25], and rectification [26]. For

[*]kheirabadinarjes@gmail.com
[†]langari@sharif.edu

all of the mentioned cases, a nonzero BCD is a requirement, which makes them fundamentally important and interesting [25]. In this paper, we calculate numerically the BCD of bilayer graphene imposed by an in-plane magnetic field and obtain an expression which shows the dependence on the components of magnetic field as long as space inversion is fulfilled.

The structure of this paper is as follows. In the next section, we review the basic notions of BCD. In Sec. III we introduce the Hamiltonian of bilayer graphene with an in-plane magnetic field. Although the magnetic field breaks time-reversal symmetry, for zero gate voltage the space-inversion symmetry is valid, which leads to an expression for BCD components with respect to the components of magnetic field. This expression shows the dominant behavior of magnetic field. We present the numerical results of our model in Sec. IV, where we investigate the dependence of BCD on the energy gap, Fermi energy, and magnetic fields, which justifies our analytic findings. We discuss some practical aspects of our results in Sec. V and conclude our finding is Sec. VI.

II. BERRY CURVATURE DIPOLE MOMENT

For an applied in-plane oscillating electric field with angular frequency ω, $\vec{E}(t) = \mathrm{Re}\{\vec{E}e^{i\omega t}\}$. Based on the Boltzmann transport approach, as mentioned in Sec. I, it has been shown that two currents in the second order of the electric field that originate from the anomalous velocity of electrons are anticipated in a crystal: $j_a = \mathrm{Re}\{j_a^0 + j_a^{2\omega}e^{2i\omega t}\}$ [5]. Here, j_a^0 is the DC response to the applied oscillating electric field, and $j_a^{2\omega}$ is the second-harmonic generation current. For 2D materials, like bilayer graphene, it has been shown that the AC and DC currents have the following forms [5,15]:

$$\begin{aligned} \vec{j}^0 &= \frac{e^3\tau}{2\hbar^2(1+i\omega\tau)}\hat{z}\times\vec{E}^*(\vec{D}\cdot\vec{E}), \\ \vec{j}^{2\omega} &= \frac{e^3\tau}{2\hbar^2(1+i\omega\tau)}\hat{z}\times\vec{E}(\vec{D}\cdot\vec{E}). \end{aligned} \tag{1}$$

In the above equations, e is the absolute value of electron charge, $e > 0$, τ is the scattering time, and $\mathbf{D}$ is the dipole moment of the Berry curvature over the occupied states, BCD, which is equal to

$$D_a = \int_k f_0(\partial_a\Omega_z), \tag{2}$$

where $\int_k \equiv \int d^2k/(2\pi)^2$ and f_0 is the equilibrium Fermi-Dirac distribution function [5]. At zero temperature, $f_0 = \Theta[\mu - \epsilon(\mathbf{k})]$, where ϵ is the energy dispersion of electrons and μ is the Fermi level. Thus, $f_0 = 1$ if $\epsilon(\mathbf{k}) < \mu$; otherwise, $f_0 = 0$. In 2D materials, the Berry curvature is a pseudoscalar that has only an out-of-plane component. Consequently, BCD is a pseudovector confined in the corresponding 2D plane and is normalized to unit length [5]. Furthermore, for 2D materials, the Berry curvature of the nth band is defined by the following equation:

$$\Omega_z^n(\mathbf{k}) = i\sum_{n'\neq n}\frac{\langle n|\partial_x\hat{H}|n'\rangle\langle n'|\partial_y\hat{H}|n\rangle - (x\leftrightarrow y)}{(\epsilon_n - \epsilon_{n'})}, \tag{3}$$

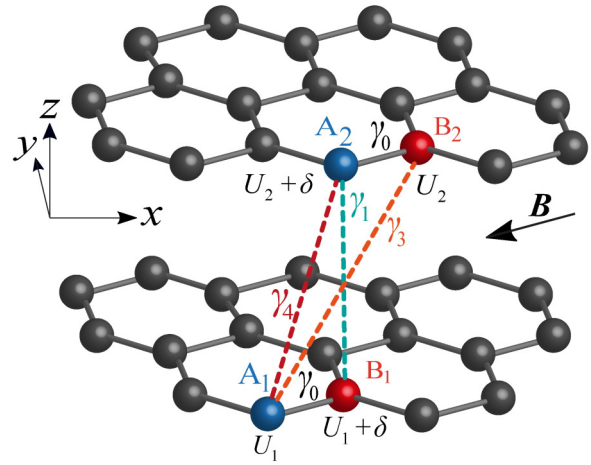

FIG. 1. The AB-stacked bilayer graphene unit cell. A_1 and B_1 atoms on the bottom layer and A_2 and B_2 on the top layer are depicted. Straight lines point out the intralayer coupling γ_0; vertical dashed lines show interlayer coupling γ_1 and skew interlayer couplings γ_3 and γ_4. The parameters U_1, U_2, and δ indicate different on-site energies.

where ϵ_n is the eigenvalue of the Hamiltonian and $\partial_{x/y} \equiv \partial_{k_x/k_y}$. It is necessary to obtain the eigenstates and eigenvalues of the Hamiltonian of bilayer graphene in a parallel magnetic field to derive the Berry curvature and its corresponding dipole. In the next section, we introduce the Hamiltonian of bilayer graphene in an in-plane steady magnetic field, and we consider the effect of the symmetry on the general form of the BCD in bilayer graphene. However, the symmetry analysis, which appears in the next section, is also valid for any 2D material with broken time-reversal symmetry while space-inversion symmetry is satisfied.

III. HAMILTONIAN AND SYMMETRY ANALYSIS

The AB-stacked bilayer graphene structure and its related parameters with a lattice constant that is equal to a and interlayer distance d are depicted in Fig. 1. According to Fig. 1, different on-site energies are U_1 and U_2 on the A_1 and B_2 sites, respectively, which are the on-site energies of the two layers. δ is the energy difference between A and B sublattices on each layer. Based on the tight-binding approximation, we have considered the full Hamiltonian of bilayer graphene with hopping parameters $\gamma_0, \gamma_1, \gamma_3$, and γ_4 and on-site energies stated in Fig. 1. The band structure of bilayer graphene for a specific set of parameters is depicted in Fig. 2. The difference in layer bias, $\Delta = U_2 - U_1$, generates a finite gap at the K point of the first Brillouin zone.

To derive the Hamiltonian of bilayer graphene in a parallel magnetic field, the in-plane magnetic field has been considered as a phase change given by a path integral of $\mathbf{A}$, the vector potential of the in-plane magnetic field. For example, to calculate the H_{AB} elements of the Hamiltonian, which are related to the γ_0 hopping parameter in the tight-binding approach, and by considering the nearest-neighbor approximation, we have assumed that each A atom has three nearest-neighbor B atoms.

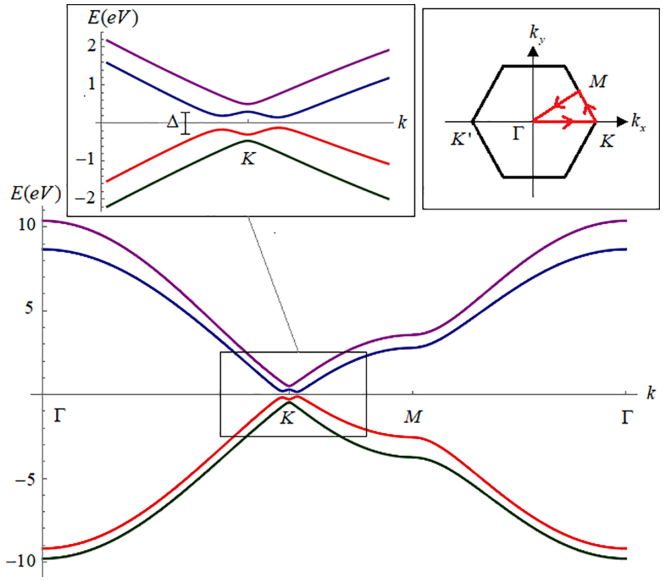

FIG. 2. The band structure of bilayer graphene along the Γ-K-M-Γ direction denoted by the red line in the right inset within the first Brillouin zone of the bilayer graphene. The left inset indicates the opening of a gap near the K point; $\Delta = U_2 - U_1 = 0.6$ eV. The parameters used to calculate the band structure are $\gamma_0 = 3.16$ eV, $\gamma_1 = 0.389$ eV, $\gamma_3 = 0.384$ eV, $\gamma_4 = 0.14$ eV, $\delta = 0.018$ eV, $a = 2.46$ Å, and $d \approx 3.3$ Å [27,28].

Consequently, H_{AB} is

$$H_{AB} = -\gamma_0 \sum_{j=1}^{3} \exp\left(i\mathbf{k}\cdot(\mathbf{R}_{Bj} - \mathbf{R}_A) - \frac{ie}{\hbar}\int_{\mathbf{R}_{Bj}}^{\mathbf{R}_A} \mathbf{A}\cdot\mathbf{d}l \right), \quad (4)$$

where $\mathbf{A}$ is chosen to be $z(B_y, -B_x)$ to keep translation symmetry in the graphene plane. The details of the derivation to reach the final Hamiltonian can be found in Ref. [29].

Hence, the 4×4 Hamiltonian of bilayer graphene in a steady parallel magnetic field in the basis of $(A_1, B_1, A_2, B_2)^T$ is [29,30]

$$H = \begin{pmatrix} U_1 & -\gamma_0 f_1(\mathbf{k}) & \gamma_4 f(\mathbf{k}) & -\gamma_3 f^*(\mathbf{k}) \\ -\gamma_0 f_1^*(\mathbf{k}) & U_1+\delta & \gamma_1 & \gamma_4 f(\mathbf{k}) \\ \gamma_4 f^*(\mathbf{k}) & \gamma_1 & U_2+\delta & -\gamma_0 f_2(\mathbf{k}) \\ -\gamma_3 f^(\mathbf{k}) & \gamma_4 f^*(\mathbf{k}) & -\gamma_0 f_2^*(\mathbf{k}) & U_2 \end{pmatrix}, \quad (5)$$

where

$$f = \exp\left(\frac{ik_y a}{\sqrt{3}}\right) + 2\exp\left(-\frac{ik_y a}{2\sqrt{3}}\right)\cos\left(\frac{k_x a}{2}\right), \quad (6)$$

$$\begin{aligned} f_1 = {} & \exp\left(\frac{ik_y a}{\sqrt{3}} + ie\frac{ad}{2\sqrt{3}\hbar}B_x\right) \\ & + \exp\left[-i\left(-\frac{k_x a}{2} + \frac{k_y a}{2\sqrt{3}}\right) - ie\frac{ad}{2\hbar}\left(\frac{B_y}{2} + \frac{B_x}{2\sqrt{3}}\right)\right] \\ & + \exp\left[-i\left(\frac{k_x a}{2} + \frac{k_y a}{2\sqrt{3}}\right) + ie\frac{ad}{2\hbar}\left(\frac{B_y}{2} - \frac{B_x}{2\sqrt{3}}\right)\right], \end{aligned} \quad (7)$$

$$\begin{aligned} f_2 = {} & \exp\left(\frac{ik_y a}{\sqrt{3}} - ie\frac{ad}{2\sqrt{3}\hbar}B_x\right) \\ & + \exp\left[-i\left(-\frac{k_x a}{2} + \frac{k_y a}{2\sqrt{3}}\right) + ie\frac{ad}{2\hbar}\left(\frac{B_y}{2} + \frac{B_x}{2\sqrt{3}}\right)\right] \\ & + \exp\left[-i\left(\frac{k_x a}{2} + \frac{k_y a}{2\sqrt{3}}\right) - ie\frac{ad}{2\hbar}\left(\frac{B_y}{2} - \frac{B_x}{2\sqrt{3}}\right)\right]. \end{aligned} \quad (8)$$

Here, $\mathbf{k}$ is the electron wave vector, and $\mathbf{B}$ is the magnetic field vector, i.e., $\mathbf{B} = (B_x, B_y, 0)$. We assume that the lower layer of the bilayer is located at $z = -d/2$ and the upper layer is at $z = +d/2$.

The time-reversal symmetry of the Hamiltonian, Eq. (5), is broken by the planar magnetic field because, apparently, $H^*(\mathbf{k}) \neq H(-\mathbf{k})$. On the other hand, $H(\mathbf{k})$ satisfies space inversion if $\mathcal{U}H(\mathbf{k})\mathcal{U}^\dagger = H(-\mathbf{k})$, where $\mathcal{U}$ is the operator swap $A_1 \leftrightarrow B_2$ and $B_1 \leftrightarrow A_2$. It can be shown that for $U_1 = U_2$ or in the absence of a gate voltage, the Hamiltonian is invariant under space inversion.

In order to resolve the symmetry properties of BCD in bilayer graphene imposed by an in-plane magnetic field, we consider the following expansion for Berry curvature (BC) in terms of the magnetic field components:

$$\Omega(k_x, k_y, B_x, B_y) = \sum_{m,n\geqslant 0} a_{m,n}(k_x, k_y) {B_x}^m {B_y}^n, \quad (9)$$

where m and n are integers and $a_{m,n}(k_x, k_y)$ are coefficients of the expansion, which are functions of momentum (k_x, k_y). Since Eq. (9) represents BC in the presence of a magnetic field, $a_{0,0}(k_x, k_y) = 0$. The Berry curvature is invariant under inversion symmetry ($\mathcal{U}$, which can be recognized as $x \to -x$ and $y \to -y$), which leads to the following constraint for the $a_{m,n}$ coefficients:

$$a_{m,n}(k_x, k_y) = (-1)^{m+n} a_{m,n}(-k_x, -k_y). \quad (10)$$

Moreover, taking into account the reflection symmetry with respect to the y axis ($x \to -x$) or the x axis ($y \to -y$) gives the following relations, respectively:

$$\begin{aligned} a_{m,n}(k_x, k_y) &= (-1)^n a_{m,n}(-k_x, k_y), \\ a_{m,n}(k_x, k_y) &= (-1)^m a_{m,n}(k_x, -k_y). \end{aligned} \quad (11)$$

According to Eq. (2), the BCD is obtained by integrating the derivatives of BC over the Brillouin zone. Making use of Eqs. (10) and (11), we show that the terms in the BCD expansion which contain both even or odd values of m and n vanish. Hence, one of the exponents (either m or n) must be odd. The proof of this statement is presented in Appendix A. Accordingly, the BCD of our model in the presence of an in-plane magnetic field has the following form:

$$D_x = B_y \int_k f_0 \sum_{m,n\geqslant 0} \frac{\partial a_{2m,2n+1}(k_x, k_y)}{\partial k_x} {B_x}^{2m} {B_y}^{2n}, \quad (12)$$

$$D_y = B_x \int_k f_0 \sum_{m,n\geqslant 0} \frac{\partial a_{2m+1,2n}(k_x, k_y)}{\partial k_y} {B_x}^{2m} {B_y}^{2n}. \quad (13)$$

Hence, whenever the inversion symmetry is satisfied in bilayer graphene, for a magnetic field in the x (y) direction a nonzero

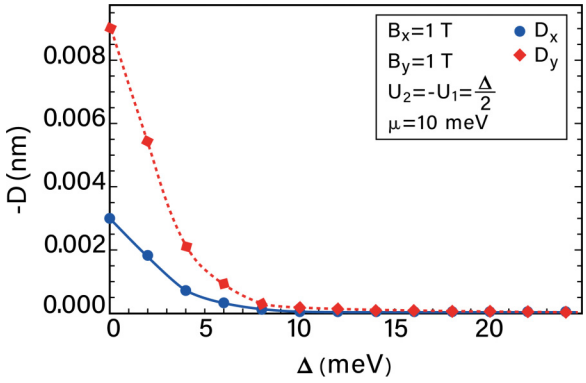

FIG. 3. The change in D_x (D_y) versus Δ (the on-site energies $U_2 = -U_1 = \Delta/2$), depicted by a solid line (dashed line) where $B_x = B_y = 1$ T. The Fermi energy is 10 meV.

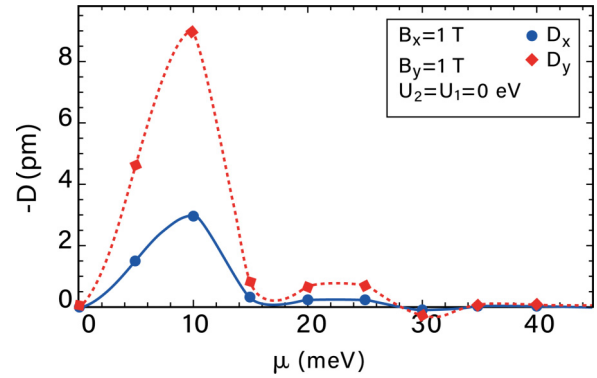

FIG. 4. The variation of the BCD versus the Fermi level μ. The solid (dashed) line depicts D_x (D_y) where $(B_x, B_y) = (0, 1)$ T [$(B_x, B_y) = (1, 0)$ T] and $U_2 = U_1 = 0$ eV. Whenever both components of the magnetic field are nonzero, $(B_x, B_y) = (1, 1)$ T, both the solid and dashed lines should be considered for D_x and D_y, respectively.

D_y (D_x) is predicted. This means that for a nonzero B_x (B_y) at B_y (B_x) = 0 T, D_y (D_x) should be the only nonzero component of BCD, which shows a linear dependence on B_x (B_y). This argument is also valid for any 2D material with broken time-reversal symmetry while space inversion symmetry is satisfied.

IV. TUNABLE BCD IN BILAYER GRAPHENE

In this section, we present numerical results for the BCD for bilayer graphene in the presence of an in-plane magnetic field. We use the following parameter values in our numerical calculations: $\gamma_0 = 3.16$ eV, $\gamma_1 = 0.389$ eV, $\gamma_3 = 0.384$ eV, $\gamma_4 = 0.14$ eV, and $\delta = 0.018$ eV; the lattice spacing is $a = 2.46$ Å, and interlayer spacing is $d \approx 3.3$ Å [27,28]. Our numerical results verify the general form of the BCD presented in Eqs. (12) and (13). In other words, as the magnetic field approaches zero, the BCD of our system vanishes regardless of the position of the Fermi energy or any applied gate voltage, so the deduced Hall effect is a genuine Hall effect. Moreover, a linear dependence of BCD on either B_x or B_y is also observed. The details of the numerical calculations are described in Appendix. B.

A. Gap-dependent BCD

Early studies on the TaAs family of Weyl semimetals showed that a zero or small gap region in the band structure leads to a large BCD [31]. The relation between the gap and BCD can be understood based on Eq. (3), where the smaller gap in the denominator causes the larger value of the BCD. Accordingly, the control on the band structure and wave functions will come out with the control on the BCD [11]. For bilayer graphene in a planar steady magnetic field, an applied in-plane magnetic field opens a gap in the band structure of bilayer graphene. For example, in the absence of any applied external gate voltage, $U_1 = U_2 = 0$ eV, and at $B_x = B_y = 1$ T, a gap of the order of 10^{-5} meV is deduced in our system. Although the amount of gap is small, it leads to a large gradient of the Berry curvature of bilayer graphene.

We plot in Fig. 3 the x and y components of the BCD of bilayer graphene for $B_x = B_y = 1$ T versus the on-site energy Δ defined by $U_2 = -U_1 = \frac{\Delta}{2}$ at chemical potential $\mu = 10$ meV.

Both components of the BCD show monotonically decreasing behavior versus Δ, where the maximum is at $\Delta = 0$, which proves the effect of the magnetic field to produce the BCD. By applying a gate voltage (presented by the on-site energies), the gap of the system is dominated by the effect of Δ rather than the gap created by the magnetic field. Increasing Δ washes out the BCD created by the magnetic field, which is clearly seen for $\Delta > 10$ meV in Fig. 3.

B. Fermi energy dependence

The Berry curvature dipole is a Fermi surface property which depends on the position of the Fermi energy. This is the motivation to obtain the BCD for different values of chemical potential. We plot in Fig. 4 both D_x and D_y versus the Fermi energy μ for $(B_x, B_y) = (1, 1)$ T and zero on-site bias $U_1 = U_2 = 0$. Both plots show nonmonotonic behavior versus μ, where the maximum BCD appears at $\mu = 10$ meV. The asymmetry between D_x and D_y for equal components of magnetic field is due to the asymmetry of the geometry of the lattice, where the x direction is along the zigzag edges. BCD is zero at $\mu = 0$, where the Fermi energy is in the middle of the gap between filled and empty bands. According to the expression for the BCD [Eq. (2)], for the latter case we would obtain zero. This means that only partially filled bands contribute to a nonzero BCD.

Moreover, we have also calculated the BCD for $(B_x, B_y) = (1, 0)$ T and $U_2 - U_1 = \Delta = 0$ eV. In agreement with our results in Sec. III, a nonzero BCD is observed only in the y direction, which falls on the dashed line in Fig. 4, while D_x is zero. If we switch the components of the magnetic fields to $(B_x, B_y) = (0, 1)$ T, a nonzero BCD in the x direction is deduced that is parallel to the zigzag edges (solid line in Fig. 4), while $D_y = 0$. The symmetry analysis of Sec. III, which led to Eqs. (12) and (13) is justified by our numerical results presented in Fig. 4. In addition, the overlap of D_x in Fig. 4 for $(B_x, B_y) = (1, 1)$ T with the case with $(B_x, B_y) = (0, 1)$ T means that in the general form of the BCD [Eqs. (12) and (13)] the linear term of expansion has the dominant effect. This is also the case of D_y for $(B_x, B_y) = (1, 1)$ and $(B_x, B_y) = (1, 0)$.

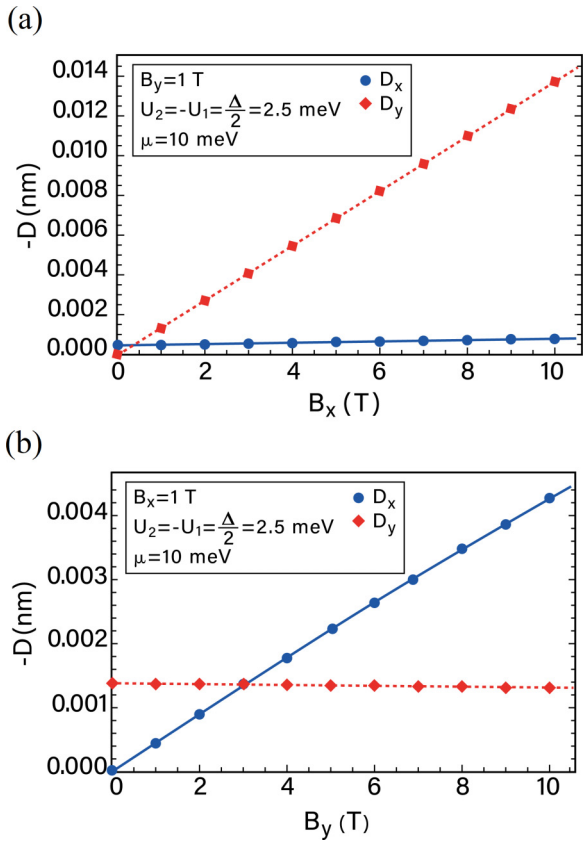

FIG. 5. The variation of D_x (D_y) versus the in-plane magnetic field is shown by a solid line (dashed line), where the Fermi energy is 10 meV and $U_2 = -U_1 = \Delta/2 = 2.5$ meV. (a) The magnetic field in the y direction is constant, $B_y = 1$ T, while B_x changes from 0 to 10 T. (b) The magnetic field in the x direction is fixed to $B_x = 1$ T, while the other component, B_y, changes form 0 to 10 T.

C. BCD dependence on the in-plane magnetic field

Here, we study the effect of a steady in-plane magnetic field on BCD for a nonzero gate voltage. It has to be mentioned that a nonzero gate potential ($\Delta \neq 0$) breaks the inversion symmetry of our model and we cannot rely on the arguments that led to Eqs. (12) and (13). Accordingly, we considered two cases at nonzero on-site energy $\Delta = 5$ meV, (a) the effect of B_x on the BCD for fixed $B_y = 1$ T and (b) the response to B_y at fixed $B_x = 1$ T.

We plot both D_x and D_y versus B_x at fixed $B_y = 1$ T and $\Delta = 5$ meV in Fig. 5(a). We observe a nonzero and almost constant value for D_x even at $B_x = 0$, which shows that it is mainly controlled by the fixed value of B_y. However, D_y shows a linear behavior versus B_x, which resembles the leading term obtained in Eq. (13).

In Fig. 5(b), the components of BCD are plotted versus B_y at constant values of $B_x = 1$ T and $\Delta = 5$ meV. Similar to the case in Fig. 5(a), D_y is nonzero and constant versus B_y, suggesting its dependence on B_x. Moreover, D_x has an almost linear dependence on B_y, which looks like the leading term of Eq. (12). It has to be mentioned that the zigzag direction of graphene is along the x axis, which breaks the symmetry by exchanging $x \leftrightarrow y$.

Although a nonzero gate voltage breaks the space-inversion symmetry of our model, the numerical results reveal that the dependence of D_x (D_y) on magnetic fields is dominated by the leading terms given in Eq. (12) [Eq. (13)].

V. DISCUSSION

An applied in-plane magnetic field has two effects on bilayer graphene: (i) it breaks the time-reversal symmetry, and (ii) the magnetic field opens a band gap, that however this band gap is small but it leads to a large BCD. A symmetry analysis based on the space-inversion symmetry concludes that the BCD depends on the components of an in-plane magnetic field, which was presented in Eqs. (12) and (13). Although a nonzero gate voltage (on-site energies) breaks the space-inversion symmetry, our numerical results in Sec. IV C indicate that the magnetic field dependence of the BCD is dominated by the first term in Eqs. (12) and (13).

We mentioned in Sec. II that a nonzero BCD leads to two types of the second-order currents, a DC one and an AC one. The magnitudes of these terms are proportional to the second-order susceptibility times a squared electric field term. Moreover, based on the Boltzmann kinetic formalism, the magnitude of the susceptibility tensor is proportional to $e^3\tau D_{x(y)}/2\hbar^2(1 + i\omega\tau)$ [5,15]. So the results are valid for an oscillating electric field caused by terahertz or microwave radiation types, where $\omega\tau \approx 1$. For a deduced $D_y = -10^{-10}$ m caused by $B_x = 8$ T and $B_y = 1$ T (presented in Fig. 5), in bilayer graphene under a planar magnetic field and considering $\tau = 0.15 \times 10^{-12}$ s, we can show that for $|E| = 10^6$ V/m and $\omega = 2.1 \times 10^{13}$ rad/s, the magnitude of the current density in bilayer graphene is 0.11 A/cm. It has to be mentioned that the linear term of conductivity leads to a larger current density compared to the quantum nonlinear term, which we discussed here. However, the nonlinear term represents the topological aspect of the model that is to be considered as the corrections on the linear term.

Higher frequencies can be studied with modifications to the Boltzmann equation via quantum kinetic theory [32–34], which could be considered in future works. Additionally, at zero magnetic field each energy band has degeneracy for spin-up and spin-down electrons. When a magnetic field is applied to the bilayer graphene, the degeneracy of the spin-up and spin-down electrons is broken by the applied magnetic field, and the energy difference between spin-up and spin-down electrons is a Zeeman energy equal to $\Delta E_z = 2S\mu_B B$, where S is the spin of an electron and μ_B is the Bohr magneton. Considering $S = 1/2$ leads to a $\Delta E_z = 5.8 \times 10^{-5}$ eV/T. Hence, for a 2 T magnetic field, we get $\Delta E_z \approx 10^{-1}$ meV. In addition, in our study, the Fermi level energy changes so that $0 \leqslant \mu \leqslant 40$ meV. According to the value of Fermi energy, we can expect the total current density produced by spin-up and spin-down electrons to increase up to two times the calculated current density.

VI. CONCLUSION

This paper represents an analytical study confirmed with numerical results of the QNLPHE in bilayer graphene, which can be controlled by an in-plane steady magnetic field in

the absence of spin-orbit coupling. The proposed strategies of a tunable BCD could also be applied to a wide range of other two-dimensional materials, such as phosphorene [35], which indicates that our findings pave the way to discover exotic nonlinear phenomena in 2D materials. We revealed a QNLPHE with a Hall voltage that is quadratic with respect to the applied electric field. The orbital-induced Berry dipole is strongly enhanced in AB-stacked bilayer graphene and reaches the nanometer scale. The aim of this work was to show that this topological effect emerges even in the complete absence of spin-orbit coupling in 2D Dirac materials, where two or more bands cross or nearly cross. Additionally, recently recognized optoelectronic and nonlinear transport experiments can give direct access to the dipole moment of the Berry curvature in nonmagnetic and noncentrosymmetric materials [25,36,37]. The predicted effects could also be utilized in applications that demand second-harmonic generation or rectification, which are used, for instance, in wireless communications, infrared detectors, and energy-harvesting applications. Moreover, such a magnetically switchable BCD may ease the observation of a broad range of quantum geometrical phenomena like the geometric properties of Bloch states in a large number of 2D materials and help in the consideration of other quantum geometrical phenomena [36,38], and the facilitation of fabrication and upscaling of the approach could allow exotic phases of matter attractive in twistronics [1].

ACKNOWLEDGMENTS

We would like to thank E. McCann, C. Ortix, and R. Asgari for fruitful discussions and useful comments. We thank the Office of Vice President for Research of Sharif University of Technology for financial support.

APPENDIX A: SYMMETRY ANALYSIS

As mentioned in the main text, Eqs. (12) and (13) are valid whenever $U_1 = U_2$, which means that the underlying system has space-inversion symmetry. Under this condition, the Berry curvature [Eq. (9)] should also obey the space-inversion symmetry of the system. Moreover, the honeycomb lattice is invariant under reflections with respect to the x or y axis. In this situation, we can show that the following identities are valid:

$$\begin{aligned} a_{m,n}(k_x,k_y){B_x}^m{B_y}^n &= a_{m,n}(k_x,-k_y)(-B_x)^m{B_y}^n \\ &= a_{m,n}(-k_x,k_y){B_x}^m(-B_y)^n \\ &= a_{m,n}(-k_x,-k_y)(-B_x)^m(-B_y)^n. \end{aligned} \tag{A1}$$

In the above equations, we have considered that under reflection with respect to the x axis $k_x \to k_x, k_y \to -k_y, B_x \to -B_x$, and $B_y \to B_y$. Similarly, under the reflection with respect to the y axis, we have $k_x \to -k_x$, $k_y \to k_y$, $B_x \to B_x$, and $B_y \to -B_y$. In addition, the inversion symmetry is given by $k_x \to -k_x, k_y \to -k_y, B_x \to -B_x$, and $B_y \to -B_y$.

According to the definition of the BCD [Eq. (2)] and the expression for Berry curvature proposed in Eq. (9), we will show that in the final expression for the BCD either m or n must be odd. Those terms which contain exponents (m, n) that are both odd or both even vanish in the final expression for the BCD. To prove this, we would like to stress that the BCD comes from an integration on the Brillouin zone (BZ) which can be considered symmetrically around the origin of $\mathbf{k}$ space. The integrand of Eq. (2) for D_x contains the following derivative:

$$\frac{\Delta\Omega}{\Delta k_x} = \frac{\Omega(k_x+\Delta k_x,k_y,B_x,B_y)-\Omega(k_x,k_y,B_x,B_y)}{\Delta k_x}. \tag{A2}$$

According to the reflection symmetry with respect to the y axis, for each occupied state with $k_x > 0$ there is a state at $-k_x$ in the BZ which gives

$$\frac{\Delta\Omega}{\Delta k_x} = \frac{\Omega(-k_x,k_y,B_x,B_y)-\Omega(-(k_x+\Delta k_x),k_y,B_x,B_y)}{\Delta k_x}. \tag{A3}$$

We rewrite the derivatives given in Eqs. (A2) and (A3) using the expression for BC [Eq. (9)]:

$$\frac{\Delta\Omega}{\Delta k_x} = \frac{\sum a_{m,n}(k_x+\Delta k_x,k_y){B_x}^m{B_y}^n - \sum a_{m,n}(k_x,k_y){B_x}^m{B_y}^n}{\Delta k_x}, \tag{A4}$$

$$\frac{\Delta\Omega}{\Delta k_x} = \frac{\sum a_{m,n}(-k_x,k_y){B_x}^m{B_y}^n - \sum a_{m,n}(-(k_x+\Delta k_x),k_y){B_x}^m{B_y}^n}{\Delta k_x}. \tag{A5}$$

In accordance with Eq. (A1), when m and n are both even and odd numbers, we have

$$a_{m,n}(k_x,k_y) = a_{m,n}(-k_x,k_y). \tag{A6}$$

Therefore, the corresponding terms (of both even and odd m, n) vanish in summing up the integration to obtain D_x. A similar explanation rules out the presence of both even and odd exponents in the final expression of D_y. That means either m or n should be an odd integer.

In the next step, we consider the contribution of those terms with odd m and even or zero n. Thus, we can assume that $m = 2k+1$ and $n = 2k'$ $(k, k' = 0, 1, 2, \dots)$, which leads to the following forms for Eqs. (A2) and (A3):

$$\frac{\Delta\Omega}{\Delta k_x} = \frac{\sum a_{2k+1,2k'}(k_x+\Delta k_x,k_y){B_x}^{2k+1}{B_y}^{2k'} - \sum a_{2k+1,2k'}(k_x,k_y){B_x}^{2k+1}{B_y}^{2k'}}{\Delta k_x}, \tag{A7}$$

$$\frac{\Delta\Omega}{\Delta k_x} = \frac{\sum a_{2k+1,2k'}(-k_x,k_y){B_x}^{2k+1}{B_y}^{2k'} - \sum a_{2k+1,2k'}(-(k_x+\Delta k_x),k_y){B_x}^{2k+1}{B_y}^{2k'}}{\Delta k_x}. \tag{A8}$$

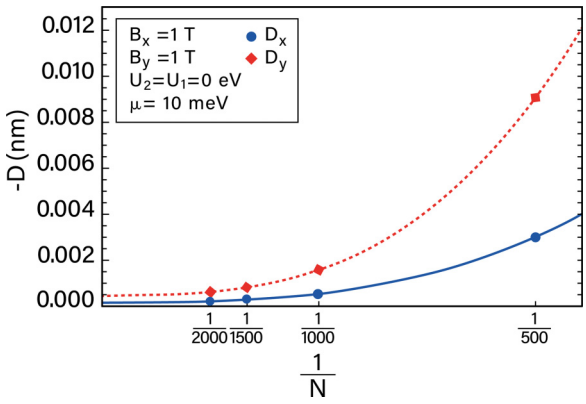

FIG. 6. The dependence of D_x and D_y versus $\frac{1}{N}$, where N is the number of mesh grids in each direction. The solid line (dashed line) represents D_x (D_y), where the other parameters are $B_x = B_y = 1$ T, $\mu = 10$ meV, and $\Delta = 0$ eV.

The application of Eq. (A1) for odd m and even n gives the subsequent identity

$$a_{2k+1,2k'}(k_x, k_y) = a_{2k+1,2k'}(-k_x, k_y). \tag{A9}$$

Consequently, the summation of Eqs. (A7) and (A8) in the integrand of D_x vanishes. The only remaining terms, which lead to nonzero D_x, are even m and odd n as presented in Eq. (12). Similar arguments verify the expression for D_y presented in Eq. (13), which completes our proof.

APPENDIX B: NUMERICAL METHOD TO CALCULATE THE BCD

The following numerical approach has been used to obtain the BCD. First, the BZ is split into a discretized mesh of $k_x(i)$ and $k_y(j)$, where $k_x(i) = \frac{2\pi i}{N}$ for $i = 0, 1, \ldots, N-1$, with similar values for $k_y(j)$. Then, based on Eq. (3), the discretized value of $\Omega_z^n(k_x(i), k_y(j))$ is assigned to a matrix of $N \times N$. This means that Ω is represented by a matrix in $\mathbf{k}$ space. The derivative of the Berry curvature in the x or y direction is derived using a finite difference method. We implemented this approach at fixed parameters of the model for different mesh grids, i.e., N. Our results show that convergence is obtained for $N \sim 2000$. We have calculated both D_x and D_y of our model at $B_x = B_y = 1$ T and $\mu = 10$ meV and in the absence of any gate voltage for different mesh grids, as shown in Fig. 6. The horizontal axis is the inverse of mesh numbers in each direction, i.e., $1/N$. However, producing data with $N = 2000$ requires a large amount of CPU time; for instance, to obtain a single point of the BCD CPU time of 14 days was spent on a machine with 80 cores. This leads us to settle on the value of $N = 500$ to produce all data points and investigate the dependence of the BCD on different parameters. Although the BCD value changes drastically from $N = 500$ to $N = 2000$, the extrapolation to $N \to \infty$ gives a nonzero result for BCD. Moreover, if we keep only the values of $N = 1000, 1500, 2000$, we observe a weaker mesh finite-size effect, which indicates that the final result will be nonzero.

[1] S.-C. Ho, C.-H. Chang, Y.-C. Hsieh, S.-T. Lo, B. Huang, T.-H.-Y. Vu, C. Ortix, and T.-M. Chen, Nat. Electron. **4**, 116 (2021).

[2] L. D. Landau and E. M. Lifshitz, *Statistical Physics* (Elsevier, Oxford, UK, 2013), Vol. 5.

[3] D. Xiao, M.-C. Chang, and Q. Niu, Rev. Mod. Phys. **82**, 1959 (2010).

[4] J. E. Moore and J. Orenstein, Phys. Rev. Lett. **105**, 026805 (2010).

[5] I. Sodemann and L. Fu, Phys. Rev. Lett. **115**, 216806 (2015).

[6] C.-X. Liu, X.-L. Qi, X. Dai, Z. Fang, and S.-C. Zhang, Phys. Rev. Lett. **101**, 146802 (2008).

[7] R. Yu, W. Zhang, H.-J. Zhang, S.-C. Zhang, X. Dai, and Z. Fang, Science **329**, 61 (2010).

[8] C.-Z. Chang, J. Zhang, X. Feng, J. Shen, Z. Zhang, M. Guo, K. Li, Y. Ou, P. Wei, L.-L. Wang *et al.*, Science **340**, 167 (2013).

[9] G. Xu, H. Weng, Z. Wang, X. Dai, and Z. Fang, Phys. Rev. Lett. **107**, 186806 (2011).

[10] A. A. Burkov, Phys. Rev. Lett. **113**, 247203 (2014).

[11] Y. Zhang, J. van den Brink, C. Felser, and B. Yan, 2D Mater. **5**, 044001 (2018).

[12] Q. Ma, S.-Y. Xu, H. Shen, D. MacNeill, V. Fatemi, T.-R. Chang, A. M. Mier Valdivia, S. Wu, Z. Du, C.-H. Hsu *et al.*, Nature (London) **565**, 337 (2019).

[13] K. Kang, T. Li, E. Sohn, J. Shan, and K. F. Mak, Nat. Mater. **18**, 324 (2019).

[14] L.-K. Shi and J. C. W. Song, Phys. Rev. B **99**, 035403 (2019).

[15] R. Battilomo, N. Scopigno, and C. Ortix, Phys. Rev. Res. **3**, L012006 (2021).

[16] G. Yin, J.-X. Yu, Y. Liu, R. K. Lake, J. Zang, and K. L. Wang, Phys. Rev. Lett. **122**, 106602 (2019).

[17] N. Wadehra, R. Tomar, R. M. Varma, R. Gopal, Y. Singh, S. Dattagupta, and S. Chakraverty, Nat. Commun. **11**, 874 (2020).

[18] A. Joshua, J. Ruhman, S. Pecker, E. Altman, and S. Ilani, Proc. Natl. Acad. Sci. USA **110**, 9633 (2013).

[19] H. X. Tang, R. K. Kawakami, D. D. Awschalom, and M. L. Roukes, Phys. Rev. Lett. **90**, 107201 (2003).

[20] M. Bowen, K.-J. Friedland, J. Herfort, H.-P. Schönherr, and K. H. Ploog, Phys. Rev. B **71**, 172401 (2005).

[21] Z. Ge, W. L. Lim, S. Shen, Y. Y. Zhou, X. Liu, J. K. Furdyna, and M. Dobrowolska, Phys. Rev. B **75**, 014407 (2007).

[22] C. Ortix, Adv. Quantum Technol. **4**, 2100056 (2021).

[23] S. V. Morozov, K. S. Novoselov, M. I. Katsnelson, F. Schedin, D. C. Elias, J. A. Jaszczak, and A. K. Geim, Phys. Rev. Lett. **100**, 016602 (2008).

[24] T. Ohta, A. Bostwick, T. Seyller, K. Horn, and E. Rotenberg, Science **313**, 951 (2006).

[25] S.-Y. Xu, Q. Ma, H. Shen, V. Fatemi, S. Wu, T.-R. Chang, G. Chang, A. M. M. Valdivia, C.-K. Chan, Q. D. Gibson *et al.*, Nat. Phys. **14**, 900 (2018).

[26] T. Ideue, K. Hamamoto, S. Koshikawa, M. Ezawa, S. Shimizu, Y. Kaneko, Y. Tokura, N. Nagaosa, and Y. Iwasa, Nat. Phys. **13**, 578 (2017).

[27] A. B. Kuzmenko, I. Crassee, D. van der Marel, P. Blake, and K. S. Novoselov, Phys. Rev. B **80**, 165406 (2009).

[28] E. McCann and M. Koshino, Rep. Prog. Phys. **76**, 056503 (2013).

[29] N. Kheirabadi, E. McCann, and V. I. Fal'ko, Phys. Rev. B **94**, 165404 (2016).
[30] N. Kheirabadi, Ph.D. thesis, Lancaster University, 2018.
[31] Y. Zhang, Y. Sun, and B. Yan, Phys. Rev. B **97**, 041101(R) (2018).
[32] S. Nandy and I. Sodemann, Phys. Rev. B **100**, 195117 (2019).
[33] C. Xiao, Z. Z. Du, and Q. Niu, Phys. Rev. B **100**, 165422 (2019).
[34] M. Farokhnezhad, R. Asgari, and D. Culcer,J. Phys. Mater. **6**, 014002 (2023).
[35] N. Kheirabadi, Phys. Rev. B **103**, 235429 (2021).
[36] R. Battilomo, N. Scopigno, and C. Ortix, Phys. Rev. Lett. **123**, 196403 (2019).
[37] C. Moulsdale, A. Knothe, and V. Fal'ko, Phys. Rev. B **101**, 085118 (2020).
[38] J.-S. You, S. Fang, S.-Y. Xu, E. Kaxiras, and T. Low, Phys. Rev. B **98**, 121109(R) (2018).